Progress in Medical Devices
eISSN: 2957-5478

Zentime

Research Article

Optimizing electrode design to minimize thermal spread in radiofrequency-induced colonic anastomosis

Lin Mao[1], Hanxiao Xue[1], Zhongxin Hu[1], Zhengyue Zhou[1], Junxian Li[1], Alfred Cuschieri[2], Chengli Song[1]

[1]Shanghai Institute for Minimally Invasive Therapy, School of Health Science and Engineering, University of Shanghai for Science and Technology, Shanghai 200093, China. [2]Institute for Medical Science and Technology, University of Dundee, DD21FD, UK.

Acknowledgements: The authors would like to acknowledge the support from the National Natural Science Foundation of China (No. 51901137, No. 51735003) and Shanghai Science and Technology Committee (No. 18441900200).

Disclosure of conflict of interest: None.

Received March 17, 2023; Accepted May 18, 2023; Published June 30, 2023

Highlights

- Three electrodes with the structure of oncave-convex, rail coupled concave-convex, and cross rail coupled con cave-convex feature were designed for radiofrequency-induced colonic anastomoses.
- The electrode with concave-convex design produced similar temperature between 'gap' and 'compressed' areas, whereas the rail coupled concave-convex exhibited the highest temperature at 'gap' and 'compressed' areas.
- The cross rail coupled concave-convex electrode, by tightly occluding upper and lower electrodes, could create uniform compression and temperature variation.

Abstract

Objective: To study temperature distribution in different electrodes and to evaluate thermal spread during colonic anastomosis induced by radiofrequency energy through finite element modeling, aiming to provide the basis for optimizing the design of new electrodes with improved effectiveness of electrosurgical welding.

Methods: Three electrodes with the feature of concave-convex (CC), rail coupled concave-convex (rail-CC), and cross rail coupled concave-convex (cross rail-CC) were designed for radiofrequency-induced serosa-to-serosa colonic anastomoses to evaluate the thermal spread process by finite element modeling using COMSOL Multiphysics. Parameters used in the modeling were set with a peak voltage of 45 V, a duty cycle of 10% and a repetition rate of 1 s. Additionally, a three-dimensional finite element model of the cross rail-CC electrode was further constructed to compare temperature variation and distribution when the voltage Fwas applied to ridges of upper electrode alternately.

Results: The electrode with CC design produced similar temperature between 'gap' and 'compressed' areas, whereas the electrode with rail-CC design exhibited the highest temperature at 'gap' and 'compressed' areas compared with those with CC and cross rail-CC designs. Moreover, the cross rail-CC electrode, by tightly occluding the upper and lower electrodes, could create uniform compression and temperature variation. When electric voltage was applied to ridges of upper electrode of the cross rail-CC electrode alternately, the temperature at 'gap' was half of that at the 'compressed' section, which was comparable to the temperature at 'compressed' area in the rail-CC electrode ($p=0.241$).

Conclusion: Alternating application of voltage to ridges of upper electrode of the cross rail-CC electrode can potentially produce an optimal fusion zone by reducing thermal damage with low 'gap' temperature while keeping the 'compressed' temperature high.

Keywords: Colonic anastomoses, radiofrequency, thermal spread, finite element modelling, electrode optimization

Address correspondence to: Chengli Song, Email: csong@usst.edu.cn Shanghai Institute for Minimally Invasive Therapy, School of Health Science and Engineering, University of Shanghai for Science and Technology, Shanghai 200093, China. Email: csong@usst.edu.cn.

Introduction

Colorectal cancer is the third most common cancer worldwide [1]. En bloc radical excision of primary tumor and regional lymph nodes by open or laparoscopic surgery, with or without neoadjuvant chemo-radiotherapy, remains the gold-standard treatment, providing cure or long-term disease-free survival with a good quality of life [2, 3]. After resection, anastomotic reconstruction to restore colorectal continuity is a general procedure to realize its physiological function in complex gastrointestinal surgery.

Hand suture, as the first-generation suture technique, was the norm for tissue reconnection and closure [4]. Nevertheless, with the development of minimally invasive technology, especially the introduction of laparoscopic surgery, mechanical staplers have been widely used in clinical practice to re-establish colonic or colorectal continuity, with the major advantages of simplifying operating procedure and shortening operating time [5, 6]. However, the technology of manual suture is time-consuming, and stapling is limited by relevant costs and some technical problems in terms of correct stapler and cartridges choice, optimal stapler-tissue interaction and proper operation, which largely determine the quality of tissue anastomosis as well as postoperative recovery [7]. Furthermore, both the two techniques inevitably introduce new wounds through mechanically puncturing and squeezing tissues together, forming a non-continuous tissue connection associated with complications such as bleeding and anastomotic leakage [8, 9].

In recent years, compressive anastomosis has been developed as the third-generation anastomosis technology with typical representatives of nickel–titanium shape memory alloy compression anastomosis clip, compression anastomosis ring, and magnetic compression anastomosis [10-14]. The significant advantage of this technology is that a continuous tissue anastomosis can be formed through a progressive tissue necrosis and abscission under a pressure of the anastomotic ring, which is expected to be evacuated through bowl movement in 7-10 days after surgery. However, the metal anastomotic ring/clip poses a significant risk of foreign body intervention to intestinal tract after surgery if the compression anastomosis clip or ring fails to be excreted from the body. Serious life-threatening complications have been reported with this technique [15]. Therefore, the compressive anastomosis technology has not been popularized in clinical practice.

Currently, there have been various attempts to explore alternative anastomotic methods to replace traditional staples or sutures. Tissue fusion based on radiofrequency (RF) energy has received considerable attention because this an innovative approach can achieve a fast, stable and continuous gastrointestinal anastomoses, and outperforms existing means of tissue reconstruction in terms of low cost, no foreign material left residue and mild inflammatory response [16-18]. Although using RF-induced thermofusion to create intestinal anastomosis represents a potentially important advance, it also poses new challenges with welded anastomoses by thermofusion including insufficient coagulation of proteins, necrosis and desquamation of parts of the circumference of the anastomotic zone, leading to dreaded complication of anastomotic leakage and causing failure of the operation. Therefore, technological research is needed to ensure reliable tissue connection and residual viability of the anastomotic zone until the tissue reconstruction is complete [19, 20].

Recent studies have indicated that the geometrical surface configuration of surgical electrode has a significant effect on the strength of anastomosis zone and thermal spread in tissues [21]. A report on heat spread during RF-induced colonic anastomoses has demonstrated that a concave-convex (CC) electrode produces less thermal damage compared with a smooth electrode by reducing ‘gap’ temperature [18]. While analytical procedures often fail to predict the interaction among RF current application, electrode configuration and thermal spread, a more reliable method is needed for this purpose. Finite element modeling (FEM), supported by numerous general-purpose codes, is one of the most efficient strategies for solving engineering problems in the field of mechanics and thermodynamics [22-24]. Considering reduced lead-times for the design and the production of electrodes for tissue welding, three different surface configurations of twin electrode plates were designed based on FEM. These configurations aim to provide a more accurate approximation of a real-world scenarios. The temperature variation and distribution when pulsed electric voltage being supplied to the electrodes were analyzed computationally. The objective was to explore the influence of structural feature on thermal spread and improve the efficiency and safety of electrosurgical RF-induced bowel anastomosis through optimizing the design of the electrode structure.

Materials and methods

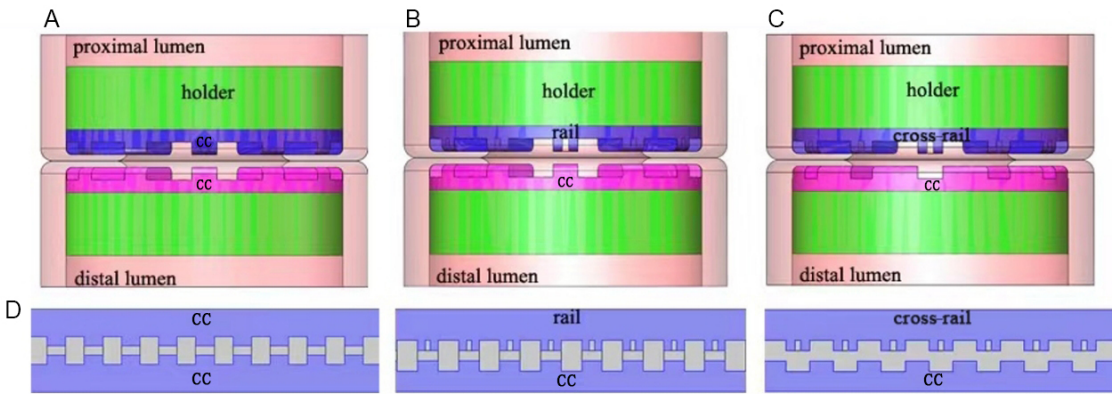

Figure 1. The omputer assisted design models and simplified 2D models. (A) CC electrode; (B) rail-CC electrode; (C) cross rail-CC electrode and (D) corresponding simplified 2D models. CC, concave-convex; rail-CC, rail coupled concave-convex; cross rail-CC, cross rail coupled concave-convex.

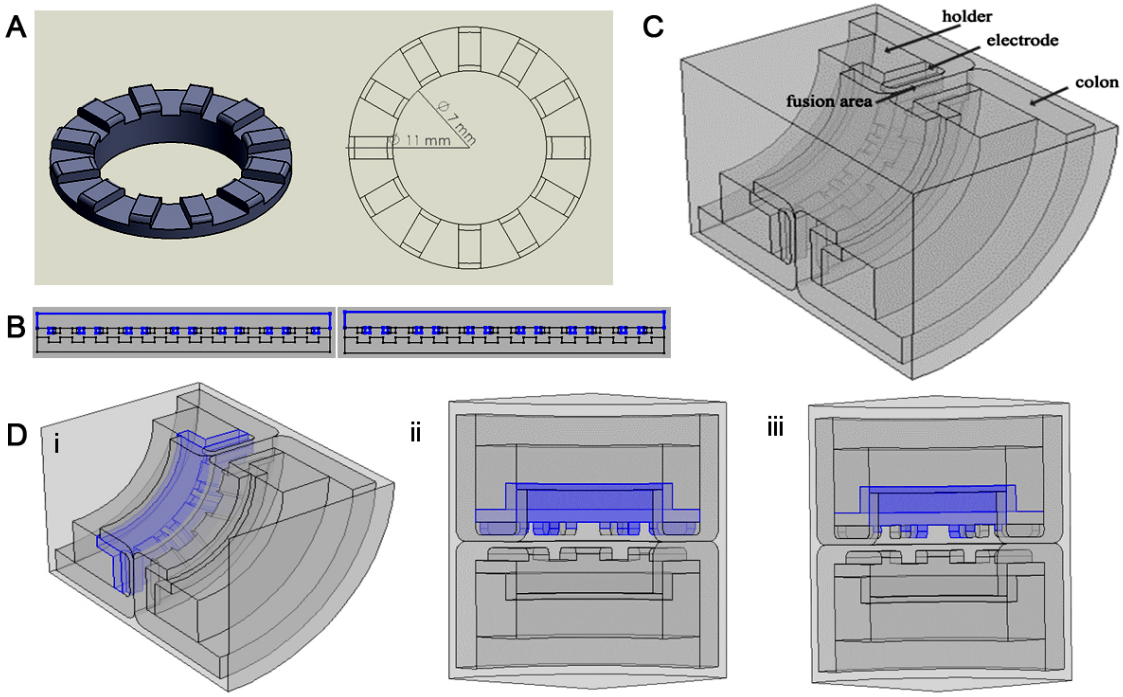

Figure 2. Specific parameters of the model. (A) The inner and external radius of electrode; (B) Electrical current applied alternately on ridges of upper electrode of the cross rail-CC electrode; (C) 3D model of the cross rail-CC electrode; (D) Electrical current was applied on the entire upper electrode (i) and on ridges of upper electrode alternately (ii, iii). CC, concave-convex; rail-CC, rail coupled concave-convex; cross rail-CC, cross rail coupled concave-convex.

2D models

Computer assisted design models of RF-induced colonic anastomoses were built (**Figure 1**), representing the results of CC electrode (**Figure 1A**), rail coupled concave-convex (rail-CC) electrode (**Figure 1B**) and cross rail coupled concave-convex (cross rail-CC) electrode (**Figure 1C**), respectively. The simplified 2D models of the corresponding electrodes are shown in **Figure 1D**.

Each electrode consists of upper and lower components which are used to place the proximal and distal bowel segments of proposed circular anastomosis and compress the colonic walls through serosa-to-serosa at certain pressures. The CC electrode contains a couple of CC plates, whereas the rail-CC and cross rail-CC electrodes both have one additional rail component besides the CC plates. Each electrode is

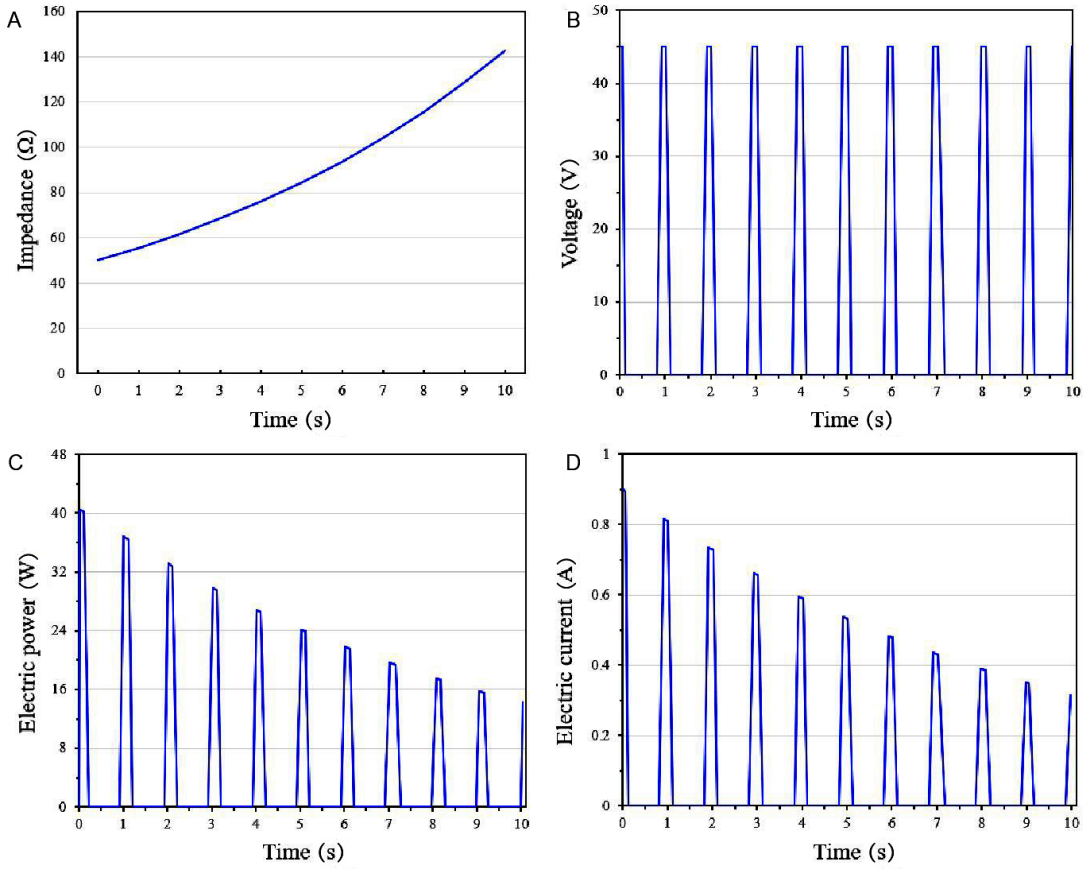

Figure 3. The electrical parameters plots during RF thermal heating simulation. (A) impedance; (B) input voltage; (C) electric power; (D) electric current. RF, radiofrequency.

designed with an inner and external radius of 7 and 11 mm, respectively (**Figure 2A**). Electrical current applied to the entire upper electrode of each electrode was 10 s. In the cross rail-CC electrode, current was also applied to ridges of upp-er electrode alternately, as illustrated in **Figure 2B**. In addition to 2D models, 3D model of the cross rail-CC electrode and current application means are presented in **Figure 2 C-D**.

Electrical power

There are two modes of RF energy with 'on' and 'off' used in electrosurgery, and the ratio of 'on' and 'off' is defined by the duty cycle. In accordance with a previous study, parameters used in FEM were 1 Hz pulsed voltage with the value of 75 V and the duty cycle of 22% for electrosurgical spleen cautery [25]. However, in order to keep enough cells alive to afford a natural wound healing, excessive thermal tissue damage should be effectively controlled during the procedure of colonic anastomoses. Thus, the power output for the FEM in this study was adjusted to 45 V with 10% duty cycle. Accordingly, the effective time applied to the entire upper electrode of each electrode was 9 s. The electrical parameter plots such as impedance plot, power plot as well as input voltage and electrical currents during heating simulation are illustrated in **Figure 3**.

Material properties

The material properties of colon are available in the referenced literature, which shows the electrical conductivity of large intestine at 470 kHz is 0.275 S/m and the permittivity is $2.43e^3$ [26]. Published work indicates that electrical conductivity decreases to a 1/4 with 55% compression, thus electrical conductivity is estimated to be 0.07 S/m when colon is compressed by electrodes [27]. The thermal conductivity (k) of large intestine is 0.54±0.03 W/ (m*k).

The electrical conductivity of biological tissue is a frequency-dependent and temperature-dependent variable, rising 1.5% per 1 °C increase until 100 °C and remaining constant at 100 °C [25, 28, 29]. Although some researches indi-

Table 1. Colon properties used in finite element modeling

	Thermal conductivity (W/m*K)	Electrical conductivity (S/m)	Density (kg/m^3)	Heat capacity at constant pressure (J/(kg*K))
Colon under compression	0.54*[1+0.015*(T^a-T0^b)], (T≤373.15 K) 0.1596, (T>373.15 K)	0.07*[1+0.015*(T-T0)], (T≤373.15 K)	1088	3655
Colon	0.1945, (T>373.15 K)	0.28*[1+0.015*(T-T0)], (T≤373.15 K) 0.6384, (T>373.15 K)		

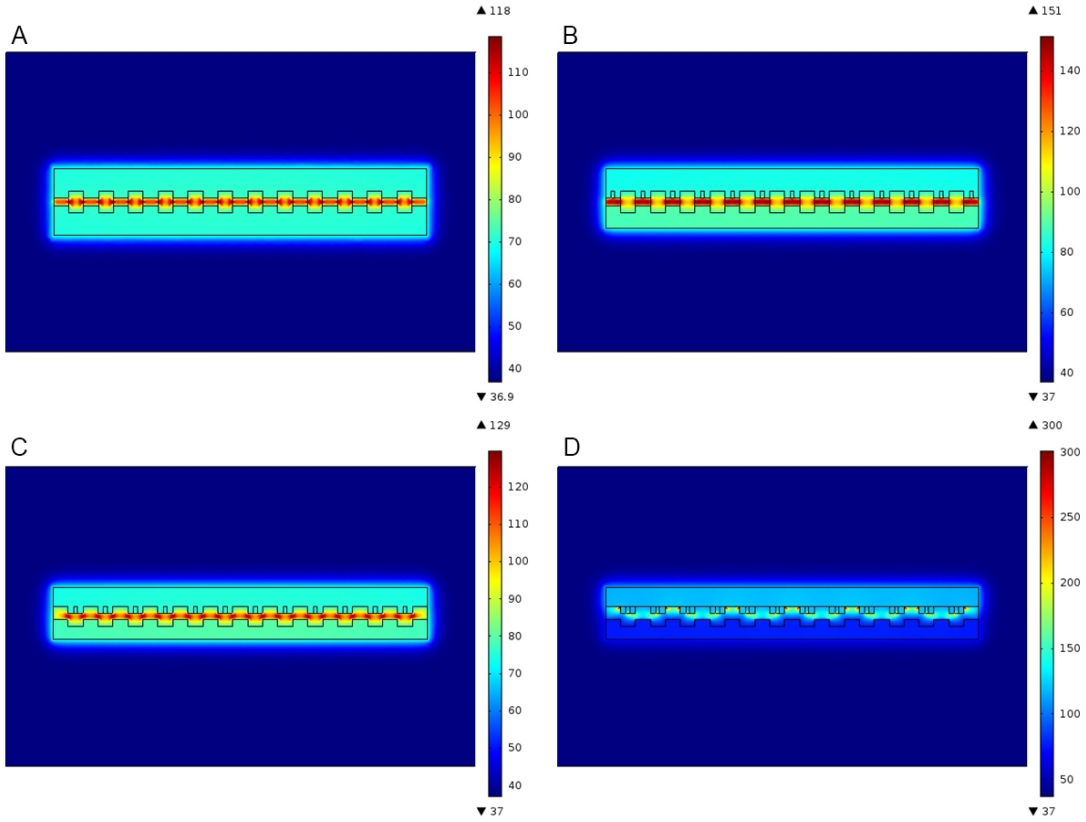

Figure 4. Temperature distributions in 2D models at 9.1 second. (A) CC electrode; (B) rail-CC electrode; (C) cross rail-CC electrode and (D) alternating cross rail-CC electrode. CC, concave-convex; rail-CC, rail coupled concave-convex; cross rail-CC, cross rail coupled concave-convex.

cate that thermal conductivity has no effect on temperature distribution, on the basis of other studies and our preliminary results, we consider that thermal conductivity is also a temperature-dependent variable, rising 1.5% per 1 °C increase until 100 °C and remaining constant at 100 °C [29-31].

The heat capacity of large intestine is 3655±64 J/(kg*K) and the density is 1088 kg/m^3 [32]. Moreover, the high humidity of abdominal cavity was simplified as liquid boundary in the model. The properties of colon are shown in **Table 1**. In addition, the holder and gaps were made of resin glass fibers, and the electrodes were made of copper.

Bio-heat transfer theory

COMSOL Multiphysics (COMSOL, UK) involving a bio-heat transfer module and an AC/DC module was utilized to analyze models. Pennes equation (as shown in equation 1) was used to calculate heat transfer in colon [33]. $\rho \cdot C\frac{\partial T}{\partial t} + \nabla \cdot (-k \cdot \nabla T) = \rho_b \cdot C_b \cdot \omega_b(T_b - T) + Q_{met} + Q_{ext}$ where ρ indicates tissue density (kg/m^3), C indicates specific heat capacity of tissue at constant pressure (J/(kg*K)), k indicates thermal conductivity (W/m*K), T is temperature (K), ρ_b indicates density of blood (kg/m^3), C_b indicates the specific heat capacity of blood (J/(kg*K)), ω_b indicates blood perfusion rate (6.4e^{-3} s^{-1}), and T_b indicates temperature of blood (K) [34]. Q_{met} indicates heat contribution from tissue metabolic activities, which can be ignored considering the short duration (10 s). Q_{ext} indicates heat source from external RF spatial heating

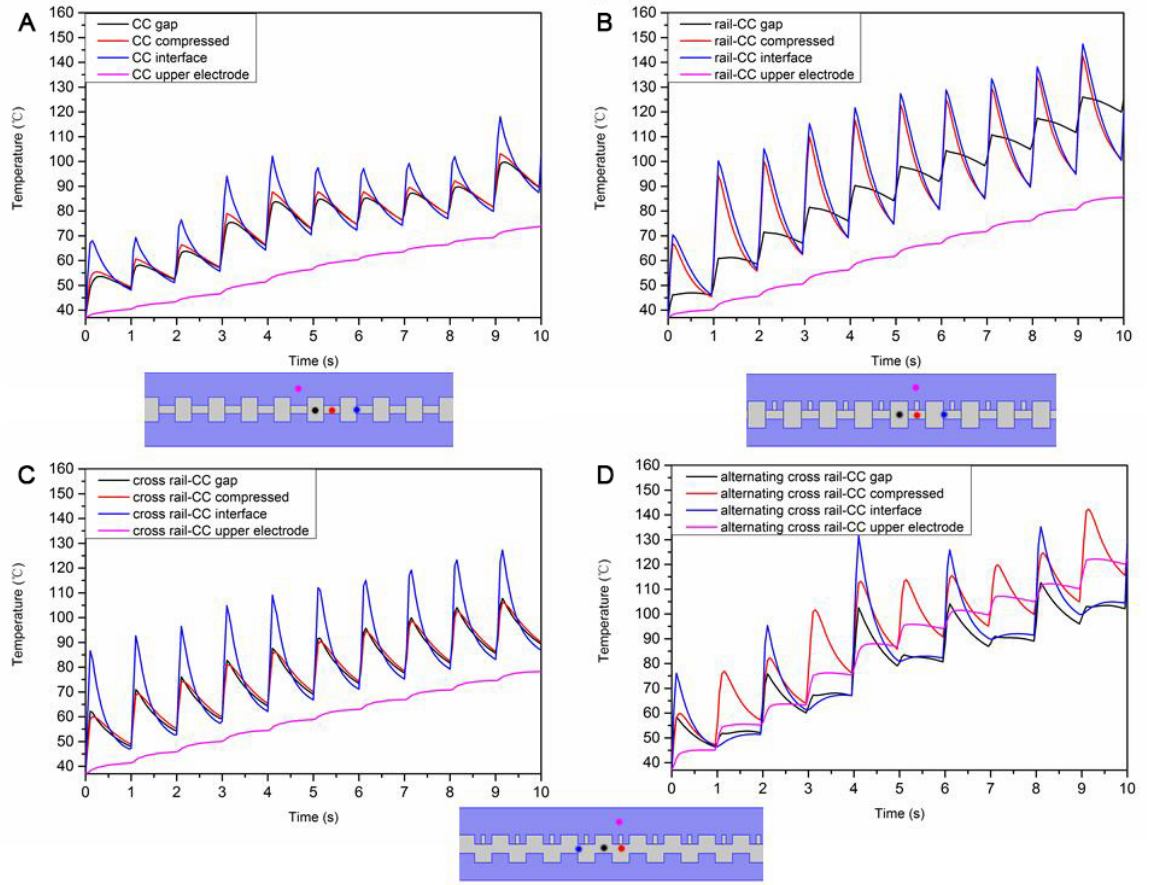

Figure 5. Real-time temperatures in 'gap', 'compressed', 'interface' and 'upper electrode' in different electrode. (A) CC electrode; (B) rail-CC electrode; (C) cross rail-CC electrode; (D) alternating cross rail-CC electrode. Black curve and red curve represent temperature of colon between gaps (plot at black point) and ridges (plot at red point), respectively. Blue curve represents temperature of colon at interface (plot at blue point). Pink curve represents temperature of upper electrode. CC, concave-convex; rail-CC, rail coupled concave-convex; cross rail-CC, cross rail coupled concave-convex.

source ($W*m^3$).

Statistical analysis

The data were processed by SPSS25.0, IBM, USA. As the simulation data were not normally distributed, non-parametric tests were used. All the data were measurement data and all the groups were compared for their temperature by the Wilcoxon rank sum test. Significance was set at $p<0.05$.

Results

Temperature distribution in 2D model

The temperature distributions in 2D models are shown in **Figure 4**. The segment of colon between ridges is defined as 'interface' area. In the CC electrode, the 'interface' area presented the highest temperature of approximating 118 °C with considerable heat spreading to gaps, whereas the temperatures in upper and lower electrodes were similar of approximating 75 °C, as shown in **Figure 4A**. In the rail-CC electrode (**Figure 4B**), the highest temperature was observed in the 'compressed' colon (the colonic segment between the protruded area of upper electrode and the corresponding area of lower electrode), reaching 151 °C. Compared to the CC electrode, less heat spread to the gaps in the rail-CC electrode, and the upper and lower electrodes reached 65 °C. When electrical voltage was applied to the entire upper electrode of the cross rail-CC prototype, heat concentrated at 'interface' between upper and lower ridges, and the temperature achieved 129 °C, obviously different from other areas of 100 °C and the electrode of 95 °C (**Figure 4C**). When voltage was applied to ridges of upper electrode alternately, the highest temperature of approximating 300 °C occurred between each ridge of upper electrode, and different temperatures could be observed between the upper

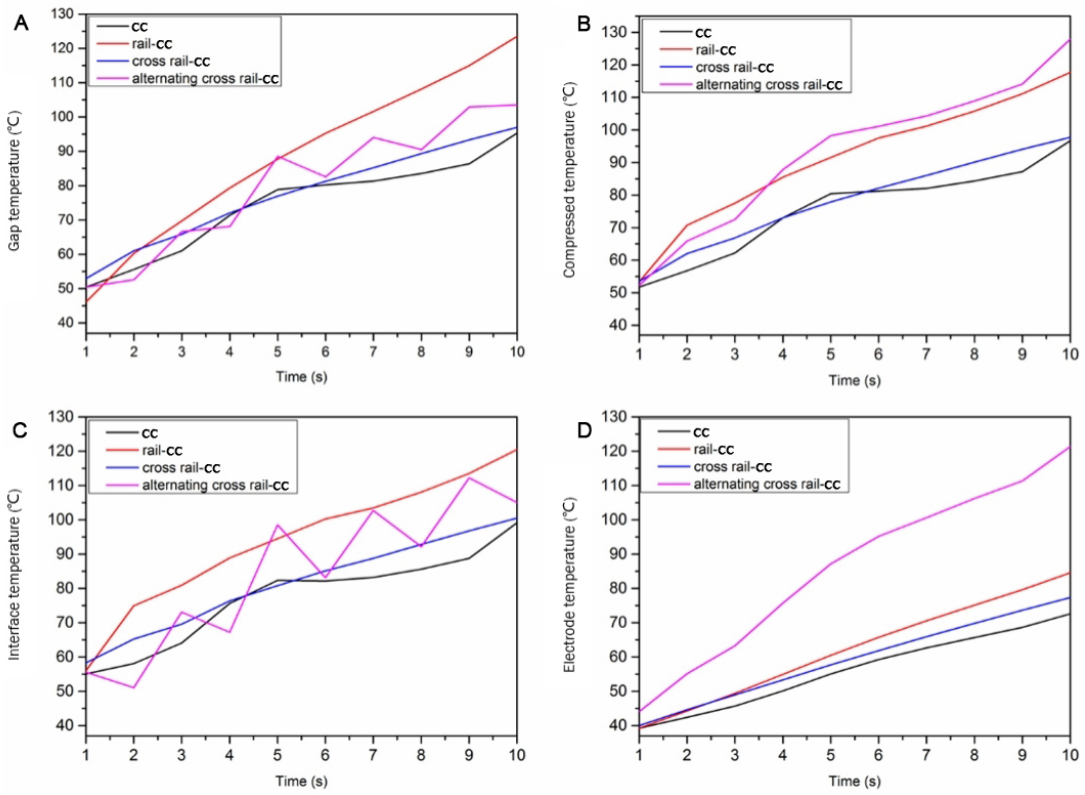

Figure 6. Temperature variations at four positions in 2-D models of the CC, rail-CC, cross rail-CC and alternating cross rail-CC electrodes. (A) 'gap'; (B) 'compressed'; (c) 'interface'; (D) 'electrode'. CC, concave-convex; rail-CC, rail coupled concave-convex; cross rail-CC, cross rail coupled concave-convex.

and lower electrodes (**Figure 4D**).

In order to explore the effect of configuration of surgical electrode on temperature variation, real-time temperatures in 'gap', 'compressed', 'interface' and 'upper electrode' were investigated, and the results are shown in **Figure 5**. In the CC, rail-CC and cross rail-CC electrodes, the temperature in 'upper electrode' exhibited a tendency of gradual rise, whereas the highest peak temperature occurred at 'interface'. The result in **Figure 5A** shows no remarkable difference in the peak temperature between 'gap' and 'compressed' in the CC electrode, whereas the peak temperature at 'interface' was slightly hig-her. Furthermore, the temperature at 'upper electrode' was less than 75 °C. As shown in **Figure 5B**, the rail-CC electrode created significantly higher 'compressed' and 'interface' peak temperatures than the temperature at 'gap'. While in **Figure 5C**, the cross rail-CC produced the highest temperature at 'interface', and similar peak temperatures were observed at 'gap' and 'compressed' area. However, the temperature at 'upper electrode' was low and similar to that of the CC electrode. In **Figure 5D**, when current was applied to ridges of upper electrode of the cross rail-CC prototype alternately, the peak temperature at 'gap' and 'interface' appeared every two seconds, whereas the peak temperature at 'compressed' region occurred every second and finally reached the highest peak temperature. Besides, the temperature at 'upper electrode' appeared to be the highest in comparison with all other groups displayed in **Figure 5A-C**.

The temperature variations at 'gap', 'compressed', 'interface' and 'electrode' in 2D models of the CC, rail-CC, cross rail-CC and alternating cross rail-CC electrodes are presented in **Figure 6**. The CC electrode created the lowest mean temperature at 'gap' (**Figure 6A**), while the alternating cross rail-CC electrode produced the highest mean temperature at 'compressed' areas of colon (**Figure 6B**). Moreover, **Figure 6B** demonstrates that the alternating cross rail-CC electrode produced considerably higher temperature at 'compressed' colon than that produced by the CC electrode ($p=0.001$). No temperature difference was found at 'compressed' area between the rail-CC and alternating cross rail-CC electrodes ($p=0.241$). It can be seen from **Figure 6C** that the CC electrode produced the lowest temperature at 'interface' sections. Although the 'interface' temperature of alternating cross rail-cc electrode was higher than that produced by the CC electrode, the

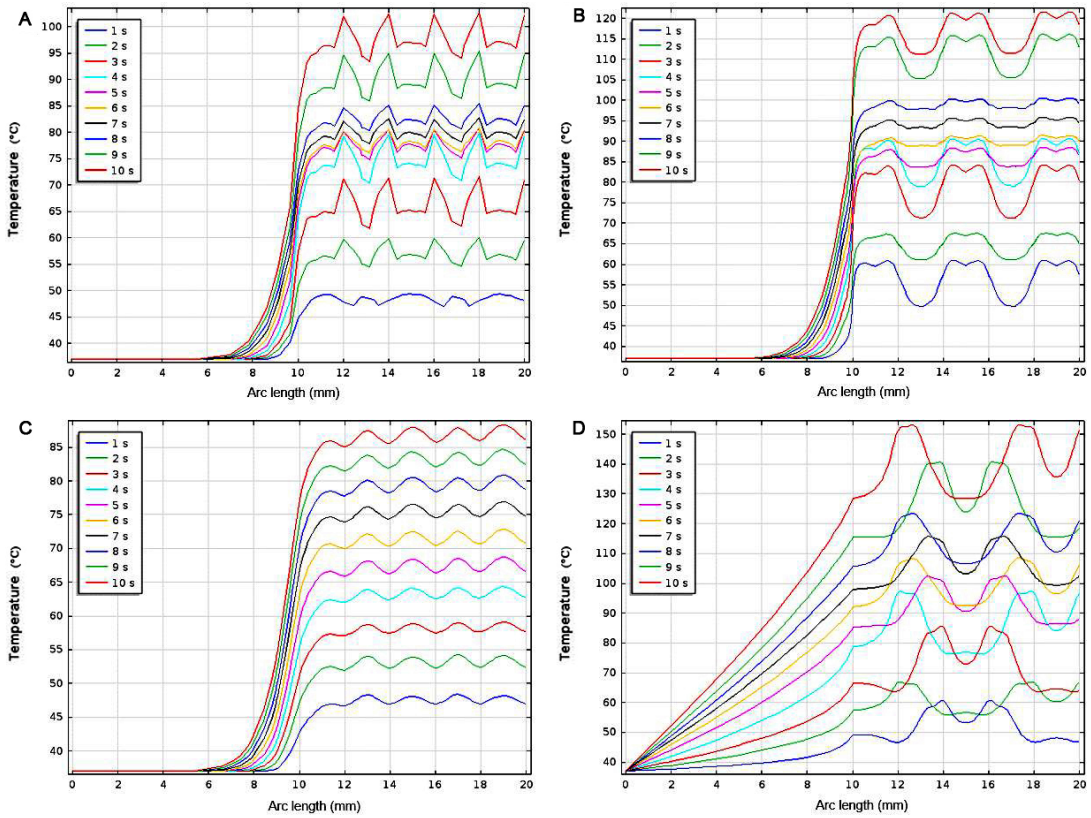

Figure 7. The temperature variations at the horizontal center line in different electrode. (A) CC electrode; (B) rail-CC electrode; (C) cross rail-CC electrode; (D) alternating cross rail-CC electrode. CC, concave-convex; rail-CC, rail coupled concave-convex; cross rail-CC, cross rail coupled concave-convex.

difference was not significant (p=0.093). Furthermore, the temperature at 'electrode' of the alternating cross rail-CC electrode was much higher than that of other electrodes, as shown in **Figure 6D**.

Based on the above results, studies were further carried out to illustrate temperatures at the horizontal center line in the fusion zone generated by each electrode, and the results are shown in **Figure 7**. The temperature curves appeared to be homogenous in the cross rail-CC electrode due to the tightly occluding upper and lower electrodes (**Figure 7C**), while both the temperature curves of the CC (**Figure 7A**) and rail-CC electrodes (**Figure 7B**) exhibited non-uniform profiles. In addition, the temperatures in the CC and rail-CC electrodes rose faster than that in the cross rail-CC electrode, and the temperatures at 'gap' and 'compressed' regions in all the three electrodes increased gradually with the extension of time. However, the increase of temperature achieved the highest in the cross rail-CC electrode when voltage was applied to ridges of upper electrode alternately (**Figure 7D**).

Temperature distribution in 3D model of the cross rail-cc electrode

Figure 8A-B shows the temperature distribution of the cross rail-CC electrode in 3D model when current was applied to the entire rail electrode, resulting in heat concentration at fusion area with a peak temperature of 114 °C at 8.1 s and 134 °C at 9.1 s, occurring every second. In contrast, as shown in **Figure 8C-D**, the highest temperature occurred at the 'interface' when current was applied to ridges alternately, and the temperature shock at fusion area occurred alternatively every two seconds.

Figure 9 displays the temperature changes at 'gap', 'compressed', 'interface', 'upper electrode' and 'lower electrode' of the cross rail-CC electrode in 3D model. Compared with 2D model, the cross rail-CC electrode produced slightly higher 'compressed' temperature when current was delivered on the entire electrode (**Figure 9A**). While in **Figure 9B**, the thermal shock at 'interface' and 'gap' appeared every seconds when current was applied to ridges alternately, differing from the periodic variation of every second at 'compressed' segment. However,

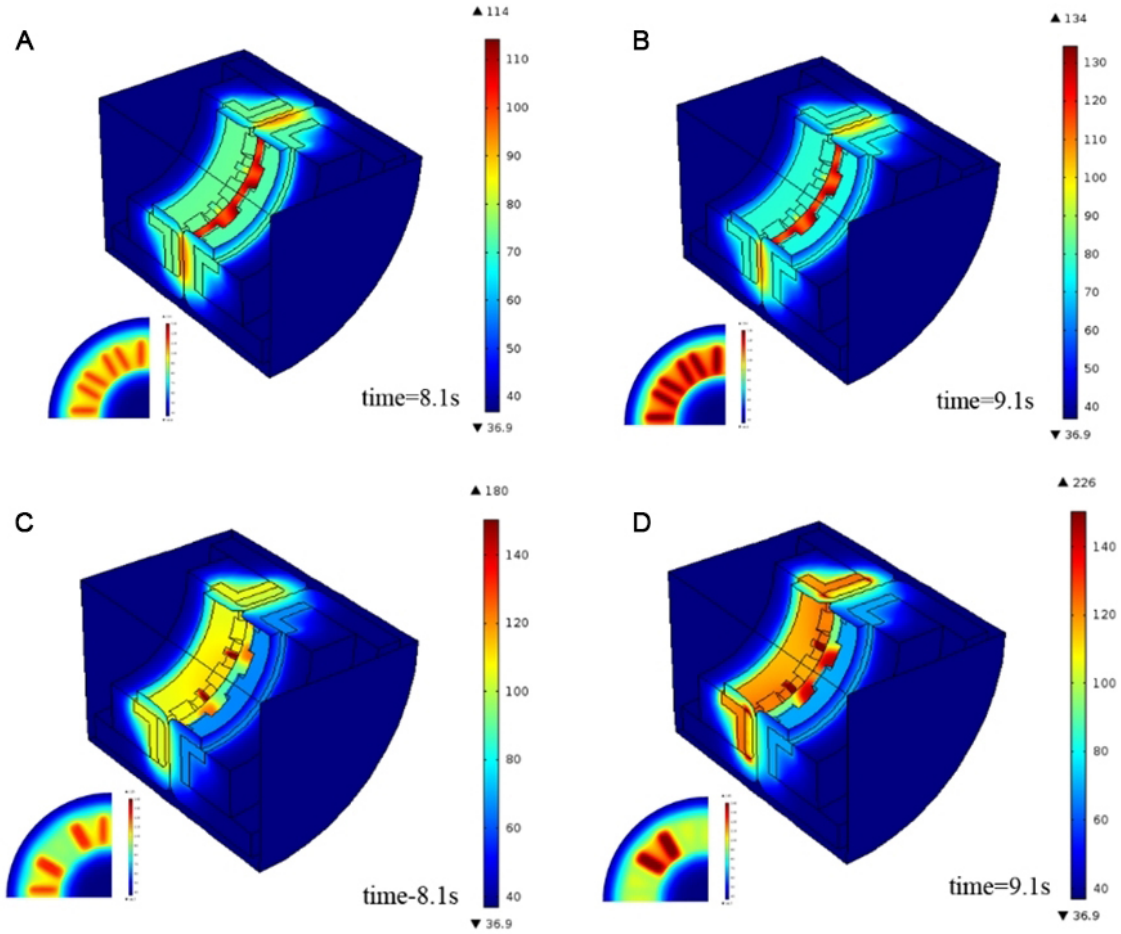

Figure 8. Temperature distributions in the cross rail-CC electrode. (A) The voltage was applied on the entire upper electrode at 8.1 s, and the peak temperature at fusion area occurred every second; (B) The voltage was applied on the entire upper electrode at 9.1 s, and the peak temperature at fusion area occurred every second; (C) The voltage was applied on the ridges of upper electrode alternatively at 8.1 s, and the temperature shock at fusion area occurred alternatively every two seconds; (D) The voltage was applied on the ridges of upper electrode alternatively at 9.1 s, and the temperature shock at fusion area occurred alternatively every two seconds. cross rail-CC, cross rail coupled concave-convex.

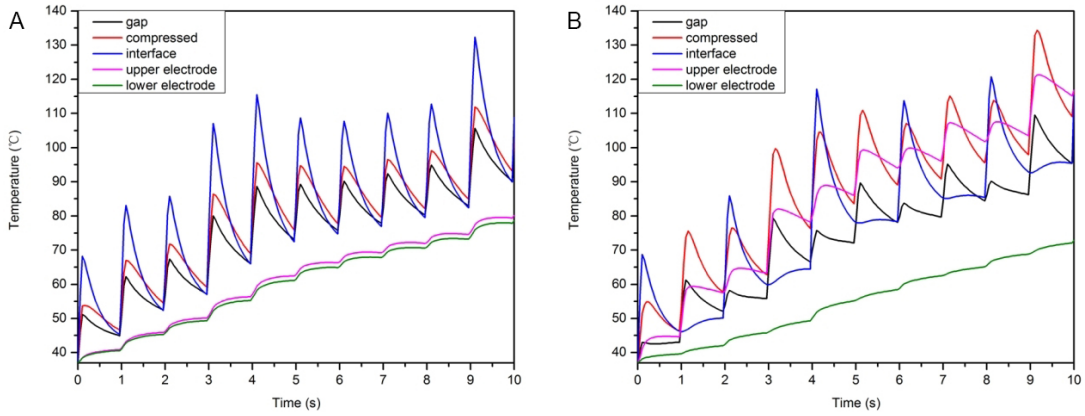

Figure 9. Temperature variations in the cross rail-CC electrode in 3D model. (A) Voltages applied on the entire rail electrode; (B) Voltage applied on ridges of upper electrode alternately. cross rail-CC, cross rail coupled concave-convex.

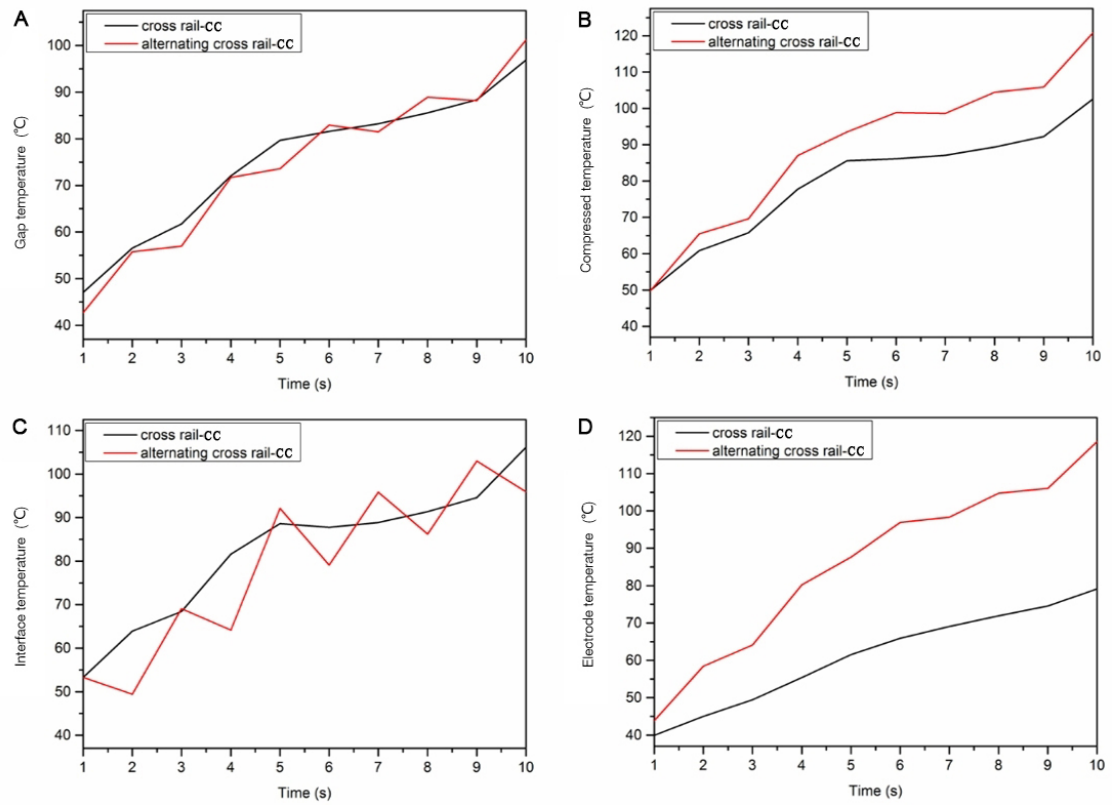

Figure 10. Mean temperatures at different positions in 3D model of the cross rail-CC electrode and alternating cross rail-CC electrode. (A) 'gap'; (B) 'compressed'; (C) 'interface'; (D) 'electrode'. cross rail-CC, cross rail coupled concave-convex.

the peak temperatures at 'gap', 'interface' and 'lower electrode' were lower, whereas temperatures at 'compressed' and 'upper electrode' were substantially higher than those in **Figure 9A**.

We finally investigated the mean temperatures at 'gap', 'compressed', 'interface' and 'upper electrode' of the cross rail-CC and alternating cross rail-CC electrodes in 3D models (**Figure 10**). No statistically difference was found in the mean temperature at 'gap' between the cross rail-CC electrode and alternating cross rail-CC electrode (**Figure 10A**), while the latter reached considerably higher 'compressed' temperature (**Figure 10B**). Additionally, the mean temperatures at 'compressed' sections in these two electrodes exhibited the same increasing tendency with the extension of time. However, a dramatic temperature changing was observed at 'interface' when voltage was applied to ridges alternately (**Figure 10C**), and obvious higher 'upper electrode' temperature in the alternating cross rail-CC electrode was observed (**Figure 10D**).

Discussion

Anastomosis is a very important surgical procedure to rebuild normal physiological structures and functions of tissues. Thermo-induced tissue fusion via RF energy has gained extensive attention clinically because this technology can achieve high-quality tissue sealing or anastomosis due to significant advantages of short operation time, less tissue damage, no foreign material residue, mild inflammation and rapid wound healing [16-18]. Biological tissue can be considered as a conductor with electrical resistance. The resistive heating generated by RF current increases the tissue temperature, causing the denaturation of proteins within the tissue. The elevated temperature results in uncoiling of the triple helical structure of collagen type I monomers and transmuting them into a random coiled mass of peptide chains. At the same time, the disconnected tissues condense to a fused mass under certain mechanical pressure [17]. In order to achieve an effective tissue bonding, on the one hand, the matching temperature should promote crosslinking of denatured collagens to ensure sufficient biomechanical strength. On the other hand, thermal effect should also be strictly controlled to minimize large area thermal damage in welding zones.

Previous studies have unveiled that configura-

tions of surgical electrodes play a crucial role in forming a successful anastomosis through effective energy delivery to achieve a satisfied biomechanical strength [18]. Meanwhile, configuration-induced change in the transport of RF current provides an opportunity to influence the conduction and diffusion of heat, which is believed to determine the thermal damage of tissue [18, 35]. In the present study, we designed three different electrodes of CC, rail-CC and cross rail-CC, to investigate the temperature variation and distribution when voltage is applied to the electrode. Our results demonstrated that similar temperature between 'gap' and 'compressed' areas was produced by the CC electrode, and the highest temperature at 'compressed' region appeared in the rail-CC electrode, whereas the temperature at 'gap' was half of that at the 'compressed' section when electric voltage was applied to ridges of upper electrode of the cross rail-CC electrode alternately. Furthermore, the temperature of upper electrode of the alternating cross rail-CC was considerably higher than that of the cross rail-CC electrode.

It is reported that when the temperature reaches about 70-80 °C, proteins within welded tissue begin to denature, initiating the process of "white coagulation". If the temperature rises to 90 °C, the cells gradually lose water content, causing tissue dehydration, but still maintain its architecture in this process [36]. Dilley et al. suggested that a sufficient sealing time (20 s) was required to form a strong vessel seal [37]. However, vessel sealing and intestinal welding have different requirements on tissue effect between. In addition to establishing a reliable tissue connection, intestinal anastomosis also needs to keep tissue activity. Therefore, the duration used in this study was 10 s considering the tissue thermal damage. It also should be pointed out that at temperatures near 100 °C, the temperature-dependent material properties experienced nonlinear phenomenon due to fluid phase changing within tissue, causing electrical conductivity increasing and impedance roll-off of target tissue. This is due to thermal dose dependency of electrical conductivity, which leads to tissue charring and dehydration, and therefore, insufficient and non-effective heating will occur.

The simulation results indicate the rail-CC electrode introduces significantly higher peak temperature at 'gap' and 'compressed' areas compared with the CC and cross rail-CC designs. In an ideal situation, high temperature is expected to appear at 'compressed' zone, which is able to achieve optimal fusion with the help from thermal energy, whereas the temperature at 'interface' and 'gap' needs to be kept low to avoid thermal damage on the tissue. When electric voltage is applied to ridges of upper electrode of the cross rail-CC electrode alternately, the temperature at 'gap' is half of which occurs at 'compressed' section, indicating that a high temperature is achieved in the fusion area and thermal spread is limited to gaps in the alternating cross rail-CC electrode.

Thus, when the findings of the present study are extrapolated to living vascularized colon, we can predict that the cross rail-CC electrode, by tightly occluding the upper and lower electrodes could create uniform compression and temperature variation, which can be an effective means to produce the optimal fusion zone. However, a lower peak temperature was observed at the fusion area. Dodde et al. has reported similar findings in a study which compared thermal spread and temperature distribution of flat with cross grooved clamps used for bipolar electrosurgery [25]. Another issue with the present cross rail-CC electrode is that the temperature difference between 'gap' and 'compressed' areas is minimal. Hence, further improvement of the cross rail-CC electrode is needed. One possibility for the improvement is to apply current on ridges alternately to form an alternating cross rail-CC electrode, in which the peak temperature at fusion area can reach as high as that created by the rail-CC electrode and considerably higher than that of the CC electrode. As compared with applying current on the entire electrode, alternating application of current can obviously decrease the peak temperature at 'gap' and enhance the temperature at 'compressed' area, thereby reducing the risk of hyperthermia for effective tissue fusion.

RF-assisted fusion of biological tissue is believed to be the result of simultaneously applied heat energy and compression pressure. Thus, the residual heating is a concern for the application of electrosurgical electrodes with complex configurations. In our study, the peak temperature occurred at 'interface' between the upper and lower ridges, or at the corner of ridges during the process of tissue anastomosis after application of RF current. Although it seems that these results do not bring the fusion temperature down, the surrounding tissue close to fusion area may be exposed to the risk of thermal damage. Thus, cooling technique should be considered while improving electrodes with complex configurations.

Besides welding electrode with optimized design, the energy output and control also play significant roles in a successful anastomosis with satisfied biomechanical strength. It was reported that a lower duty cycle could lead to a decrease in the effective RF power [38]. Therefore, we estimated a probable duty cycle of 10% for colonic anastomoses in our FEM considering that the duration of heating process required for the unfolding of helical structure and denaturation of collagen is about 0.1 s. Obviously, there are many limitations in the current study, further research needs to be carried out to realize such a dreaming technology with improved mechanical design, control algorithms and closed-loop control system. Necessary experimental verifications also have to be developed to obtain more accurate technical parameters that mainly affect the quality of colonic fusion.

Conclusion

In this study, three different electrodes characterized with the architectural features of CC, rail-CC and cross rail-CC were designed to investigate the rule of temperature diffuse after applying pulsed electric voltage in FEM models. Our results demonstrate the importance of incorporating electrode geometry in temperature variation and distribution of bowel anastomosis based on RF energy. The CC electrode produced similar temperature between 'gap' and 'compressed' areas, whereas the rail-CC electrode exhibited the highest temperature at 'gap' and 'compressed' areas compared with the CC and cross rail-CC electrodes. Obviously, the cross rail-CC electrode displays a low temperature at 'gap' and a high temperature in 'compressed' section, which is a desirable case of temperature distribution for thermo-induced tissue fusion via RF energy.

In summary, alternating application of current to the cross rail-CC electrode appears to be the optimal option for safe colonic anastomoses without excessive thermal spread. The results in this study may provide guidance on the design of electrodes for effective tissue fusion and may also direct the future selection of welding parameters for bowel anastomoses based on RF energy.

References

[1] Goodarzi E, Beiranvand R, Mosavi-Jarrahi A, et al. Incidence and Mortality Worldwide Common cancers in males and Human Development Index (HDI). J Contemp Med Sci 2020;5:281-303.

[2] Kubota Y, Okuyama T, Oi H, et al. Comparison of postoperative plasma D-dimer levels between patients undergoing laparoscopic resection and conventional open resection for colorectal cancer. Asian J Endosc Surg 2020;13(4):498-504.

[3] Watanabe J, Ishibe A, Suwa H, et al. Long-term Outcomes of a Randomized Controlled Trial of Single-incision Versus Multi-port Laparoscopic Colectomy for Colon Cancer. Ann Surg 2021;273(6):1060-1065.

[4] Al-Kattan K, Cattalani L, Goldstraw P. Bronchopleural fistula after pneumonectomy with a hand suture technique. Ann Thorac Surg 1994;58(5):1433-1436.

[5] Firat YD, Erol MF. Safe use of vascular stapling devices during laparoscopic cholecystectomy in cases with enlarged cystic canal. Eur Res J 2020.

[6] Hayashibe, Akira. The comparison of clinical results between hand suturing and mechanical stapling for gastrojejunostomy and jejunojejunostomy after SSPPD. Int J Surg 2013;11(2):161-163.

[7] Zanghì S, Siboni S, Asti E, et al. Endoscopic stapling versus laser for Zenker diverticulum: a retrospective cohort study. Eur Arch Otorhinolaryngol 2021;278(7):2625-2630.

[8] Balciscueta Z, Uribe N, Caubet L, et al. Impact of the number of stapler firings on anastomotic leakage in laparoscopic rectal surgery: a systematic review and meta-analysis. Tech Coloproctol 2020;24(9):919-925.

[9] Tao K, Gao J. Risk factors for anastomotic leakage after rectal cancer surgery. Chin J Gastrointest Surg 2018;21:384-387.

[10] Kusnierz K, Lekston Z, Zhavoronkov D, et al. A nickel-titanium memory-shape device for gastrojejunostomy: comparison of the compression anastomosis clip and a hand-sewn anastomosis. J Surg Res 2014;187(1):94-100.

[11] Koo EJ, Choi HJ, Woo JH, et al. Anastomosis by use of compression anastomosis ring (CAR™ 27) in laparoscopic surgery for left-sided colonic tumor. Int J Colorectal Dis 2012;27(3):391-396.

[12] Lu Z, Peng J, Li C, et al. Efficacy and safety of a NiTi CAR 27 compression ring for end-to-end anastomosis compared with conventional staplers: A real-world analysis in Chinese colorectal cancer patients. Clinics 2016;71(5):264-270.

[13] Jamshidi R, Stephenson JT, Clay JG, et al. Magnamosis: magnetic compression anastomosis with comparison to suture and staple techniques. J Pediatr Surg 2009;44(1):222-228.

[14] Jiang XM, Yamamoto K, Tsuchiya T, et al. Magnetic compression anastomosis for biliary obstruction after partial hepatectomy. Endoscopy 2018;50(6):144-145.
[15] Thiede A, Geiger D, Dietz UA, et al. Overview on Compression Anastomoses: Biofragmentable Anastomosis Ring Multicenter Prospective Trial of 1666 Anastomoses. World J Surg 1998;22(1):78-87.
[16] Arya S, Hadjievangelou N, Lei S, et al. Radiofrequency-induced small bowel thermofusion: an ex vivo study of intestinal seal adequacy using mechanical and imaging modalities. Surg Endosc 2013;27(9):3485-3496.
[17] Holmer C, Winter H, Nagel A, et al. Bipolar radio-frequency-induced thermofusion of intestinal tissue – In vivo evaluation of a new fusion technique in an experimental study. Int J Hyperthermia 2016;32(5):583-586
[18] Zhao L, Song C, Wang Z, et al. Novel concave-convex electrode for colonic anastomoses by radiofrequency thermo-fusion. Surg Endosc 2015;29(7):1809-1816.
[19] Lim C, Goldin RD, Elson DS, et al. In vivo thermography during small bowel fusion using radiofrequency energy. Surg Endosc 2010;24(10):2465-2474.
[20] Merlini, l'Héritier, Siproudhis, et al. Sphincter-sparing surgery for complex anal fistulas: radiofrequency thermocoagulation of the tract is of no help. Colorectal Dis 2019;21(8):961-966.
[21] Wang M, Zhang Y, Xue P, et al. Optimized SEEG-guided radiofrequency thermocoagulation in the treatment of pediatric hypothalamic hamartomas. Seizure 2021;86:102-108.
[22] Nazir U, Saleem S, Nawaz M, et al. Three-dimensional heat transfer in nonlinear flow: a FEM computational approach. J Therm Anal Calorim 2020;140:2519-2528.
[23] Sliseris J, Gaile L, Pakrastins L. Extended multiscale FEM for design of beams and frames with complex topology. Appl Math Model 2019;69:77-92.
[24] Yang CH, Li W, Chen KR. Determination of Tissue Thermal Conductivity as a Function of Thermal Dose and Its Application in Finite Element Modeling of Electrosurgical Vessel Sealing. IEEE T Bio-Med Eng 2020;67(10):2862-2869.
[25] Dodde RE, Miller SF, Geiger JD, et al. Thermal-Electric Finite Element Analysis and Experimental Validation of Bipolar Electrosurgical Cautery. J Manuf Sci E 2008;130:241-248.
[26] Hasgall PA, Neufeld E, Gosselin MC, et al. It is Database for thermal and electromagnetic parameters of biological tissues. J Cell Biol 2012;93:170.
[27] Dodde RE, Bull JL, Shih AJ. Bioimpedance of soft tissue under compression. Physiol Meas 2012;33(6):1095-1109.
[28] Haemmerich D, Chachati L, Wright AS, et al. Hepatic radiofrequency ablation with internally cooled probes: effect of coolant temperature on lesion size. IEEE T Bio-Med Eng 2003;50(4):493-500.
[29] Jo B, Aksan A. Prediction of the extent of thermal damage in the cornea during conductive keratoplasty. J Therm Biol 2010;35:167-174.
[30] Pujari AK, Prasad B, Sitaram N. Effect of Thermal Conductivity on Nozzle Guide Vane Internal Surface Temperature Distribution. Int J Turbo Jet Eng 2018;38(2):135-151.
[31] Baldwin SA, Pelman A, Bert JL. A heat transfer model of thermal balloon endometrial ablation. Ann Biomed Eng 2001;29(11):1009-1018.
[32] Cameron, John. Physical Properties of Tissue. A Comprehensive Reference Book, edited by Francis A. Duck. Med Phys 1991;18:834.
[33] Pennes HH. Analysis of tissue and arterial blood temperatures in the resting human forearm. J Appl Physiol 1998;85(1):5-34.
[34] Williams LR, Leggett RW. Reference values for resting blood flow to organs of man. Clin Phys Physiol Meas 1989;10(3):187-217.
[35] Ciovati G, Cheng G, Pudasaini U, et al. Multi-metallic conduction cooled superconducting radio-frequency cavity with high thermal stability. Supercond Sci Tech 2020;33(7):468-472.
[36] Wu MP, Ou CS, Chen SL, et al. Complications and Recommended Practices for Electrosurgery in Laparoscopy. Am J Surg 2000;179(1):67-73.
[37] Dilley AV, Friend MG, Morris DL. An experimental study of optimal parameters for bipolar electrocoagulation. Gastrointest Endosc 1995;42(1):27-30.
[38] Zhang X, Wagatsuma K. Emission characteristics of 6.78-MHz radio-frequency glow discharge plasma in a pulsed mode. Spectrochim Acta B 2017;133(2):72-80.